Journal of Molecular Catalysis A: Chemical 321 (2010) 1–9

Contents lists available at ScienceDirect

Journal of Molecular Catalysis A: Chemical

journal homepage: www.elsevier.com/locate/molcata

Editor's Choice paper

Synthesis and catalytic activity of new Gd_2BiSbO_7 and Gd_2YSbO_7 nanocatalysts

Jingfei Luan[a,*], Kun Ma[a], Bingcai Pan[a], Yongmei Li[b], Xiaoshan Wu[c], Zhigang Zou[d]

[a] State Key Laboratory of Pollution Control and Resource Reuse, School of the Environment, Nanjing University, Hankou Road 22, Jiangsu, Nanjing 210093, People's Republic of China
[b] State Key Laboratory of Pollution Control and Resource Reuse, School of the Environment, Tongji University, Shanghai 200092, People's Republic of China
[c] National Laboratory of Solid State Microstructures, Nanjing University, Nanjing 210093, People's Republic of China
[d] Eco-Materials and Renewable Energy Research Center, Nanjing University, Nanjing 210093, People's Republic of China

ARTICLE INFO

Article history:
Received 26 September 2009
Received in revised form 31 January 2010
Accepted 1 February 2010
Available online 6 February 2010

Keywords:
Gd_2BiSbO_7
Gd_2YSbO_7
Structural property
Photocatalytic degradation
Visible light irradiation

ABSTRACT

Gd_2BiSbO_7 and Gd_2YSbO_7 were prepared for the first time and the structural and photocatalytic properties of Gd_2BiSbO_7 and Gd_2YSbO_7 were investigated. The results showed that Gd_2BiSbO_7 and Gd_2YSbO_7 crystallized with the pyrochlore-type structure, cubic crystal system by space group *Fd*3*m*. The lattice parameters *a* for Gd_2BiSbO_7 and Gd_2YSbO_7 were 10.70352(7) and 10.65365(1) Å, respectively. The band gaps of Gd_2BiSbO_7 and Gd_2YSbO_7 were estimated to be 2.081 and 2.396 eV, respectively. The photocatalytic degradation of rhodamine B (RhB) over Gd_2BiSbO_7 and Gd_2YSbO_7 was investigated under visible light irradiation. The results showed that Gd_2YSbO_7 and Gd_2BiSbO_7 owned higher catalytic activity compared with Bi_2InTaO_7. Moreover, Gd_2YSbO_7 showed higher catalytic activity compared with Gd_2BiSbO_7 for RhB photocatalytic degradation. The photocatalytic RhB degradation followed the first-order reaction kinetics, the apparent first-order rate constant *k* being 0.01766, 0.01906 and 0.00318 min^{-1} with Gd_2BiSbO_7, Gd_2YSbO_7 and Bi_2InTaO_7, respectively. Complete removal of RhB was realized after visible light irradiation for 230 and 240 min with Gd_2YSbO_7 and Gd_2BiSbO_7. The reduction of the total organic carbon and the evolution of CO_2 revealed complete removal of RhB during the photocatalytic process by Gd_2YSbO_7 and Gd_2BiSbO_7. The possible photocatalytic degradation pathway of RhB was revealed under visible light irradiation.

1. Introduction

Novel photocatalysts have attracted extensive attention from both academic and industrial organizations [1–26] since the first manuscript of Honda and Fujishima in 1972, where electrochemical photolysis of water at a semiconductor electrode was reported [1]. Recently, some photocatalysts with different structures have been prepared to investigate the effective utilization of solar energy [12,17,27–35]. In particular, many scientific investigations on the photocatalytic degradation of aqueous organic contaminants have been reported [15,36–62]. Within all categories of dyestuffs, rhodamine B is one of the most important representatives of xanthene dyes, and it is widely used as a photosensitizer, a quantum counter and an active medium in dye lasers, etc. [63,64]. However, rhodamine B is resistant to biodegradation and direct photolysis, and as a N-containing dye, it undergoes natural reductive anaerobic degradation, yielding potentially carcinogenic aromatic amines [27,65]. Therefore, it is urgent and important to investigate the degradation of rhodamine B. Rhodamine B is often used as a probe contaminant to evaluate the activity of a photocatalyst both under ultraviolet light [66–70] and under visible light [27,71–75]. Within the context of visible light photodegradation of rhodamine B we may outline the work of Zhu et al. [27] utilizing Bi_2WO_6, the work of Li and Ye [71] utilizing $Pb_3Nb_4O_{13}$/fumed SiO_2 composite and the work of Zhao et al. [72] who used TiO_2 nanostripe.

Visible light photodegradation phenomena are not limited to titanium dioxide. In fact other oxides, and in particular mixed oxides such as $A_2B_2O_7$ compounds are often considered to have photocatalytic properties. In our previous work [45], we have found that Bi_2InTaO_7 crystallizes with the pyrochlore-type structure, acts as a photocatalyst under visible light irradiation and seems to have potential for activity improvement upon modification of its structure. Along this line, it can be postulated that substitution of Ta^{5+} by Sb^{5+}, substitution of In^{3+} by Bi^{3+} or substitution of In^{3+} by Y^{3+}, and substitution of Bi^{3+} by Gd^{3+} in this compound may lead to an increase about carriers concentration, which may result in improved photocatalytic properties.

Gd_2YSbO_7 and Gd_2BiSbO_7 are semiconductor compounds that were never synthesized before. The similarity between the molecular composition of these two compounds and other $A_2B_2O_7$ compounds suggests that these two compounds may possess photocatalytic properties under visible light irradiation and may be to those of other members of the family. This contribution reports the preparation and characterization of Gd_2YSbO_7 and

* Corresponding author. Tel.: +86 0 13585206718; fax: +86 0 2583707304.
E-mail address: jfluan@nju.edu.cn (J. Luan).

1381-1169/$ – see front matter.
doi:10.1016/j.molcata.2010.02.003

Gd_2BiSbO_7. The structural, photophysical and photocatalytic properties of Gd_2YSbO_7 and Gd_2BiSbO_7 were investigated in detail. A comparison among the photocatalytic properties of Gd_2YSbO_7, Gd_2BiSbO_7 and Bi_2InTaO_7 was completed in order to elucidate the structure–photocatalytic activity relationship in these newly synthesized compounds.

2. Experimental

The novel photocatalysts were synthesized by a solid-state reaction method. Sb_2O_5, Gd_2O_3, Bi_2O_3, Y_2O_3, In_2O_3, and Ta_2O_5 with purity of 99.99% (Sinopharm Group Chemical Reagent Co., Ltd., Shanghai, China) were used as starting materials. All powders were dried at 200 °C for 4 h before synthesis was performed. In order to synthesize Gd_2YSbO_7, the precursors were stoichiometrically mixed, then pressed into small columns and put into an alumina crucible (Shenyang Crucible Co., Ltd., China). Finally, calcination was carried out at 1320 °C for 50 h in an electric furnace (KSL 1700X, Hefei Kejing Materials Technology Co., Ltd., China). Similarly, Gd_2BiSbO_7 was prepared by calcination at 1040 °C for 30 h, and Bi_2InTaO_7 was prepared by calcination at 1050 °C for 46 h. The crystal structures of Gd_2YSbO_7 and Gd_2BiSbO_7 were analyzed by the powder X-ray diffraction method (D/MAX-RB, Rigaku Corporation, Japan) with CuKα radiation (λ = 1.54056). The data were collected at 295 K with a step-scan procedure in the range of 2θ = 10–100°. The step interval was 0.02° and the time per step was 1.2 s. The chemical composition of the compound was determined by scanning electron microscope-X-ray energy dispersion spectrum (SEM-EDS, LEO 1530VP, LEO Corporation, Germany) and X-ray fluorescence spectrometer (XFS, ARL-9800, ARL Corporation, Switzerland). The oxygen content, Bi^{3+} content, Gd^{3+} content, Y^{3+} content and Sb^{5+} content of Gd_2YSbO_7 and Gd_2BiSbO_7 were determined by X-ray photoelectron spectroscopy (XPS, ESCALABMK-2, VG Scientific Ltd., UK). The chemical composition within the depth profile of Gd_2YSbO_7 or Gd_2BiSbO_7 was examined by the argon ion denudation method when X-ray photoelectron spectroscopy was used. The optical absorption of Gd_2YSbO_7 and Gd_2BiSbO_7 was analyzed with an UV–vis spectrophotometer (Lambda 40, PerkinElmer Corporation, USA). The surface areas were measured by the Brunauer–Emmett–Teller (BET) method (MS-21, Quantachrome Instruments Corporation, USA) with N_2 adsorption at liquid nitrogen temperature. The particle sizes of the photocatalysts were measured by malvern's mastersize-2000 particle size analyzer (Malvern Instruments Ltd., UK). The particle morphology was measured by transmission electron microscope (Tecnal F20 S-Twin, FEI Corporation, USA).

The photocatalytic degradation of rhodamine B (RhB) (Tianjin Kermel Chemical Reagent Co., Ltd.) was performed with 0.8 g Gd_2YSbO_7, Gd_2BiSbO_7 or Bi_2InTaO_7 powder suspended in 300 mL 0.0293 mM RhB solution in a pyrex glass cell (Jiangsu Yancheng Huaou Industry, China). Before irradiation, the suspensions were magnetically stirred in the dark for 45 min to ensure establishment of an adsorption/desorption equilibrium among Gd_2YSbO_7, Gd_2BiSbO_7, Bi_2InTaO_7, the RhB dye and atmospheric oxygen. The photocatalytic reaction system consisted of a 300 W Xe arc lamp with the main emission wavelength at 436 nm (Nanjing JYZCPST Co., Ltd.), a magnetic stirrer and a cut-off filter (λ > 400 nm, Jiangsu Nantong JSOL Corporation, China). The Xe arc lamp was surrounded by a quartz jacket and was positioned within the inner part of a photoreactor quartz vessel (5.8 cm in diameter and 68 cm in length), through which a suspension of RhB and photocatalyst was circulated. An outer recycling water glass jacket maintained a near constant reaction temperature (22 °C), and the solution was continuously stirred and aerated. 2 mL aliquots were sampled at various time intervals. The incident photon flux I_o measured by a radiometer (Model FZ-A, Photoelectric Instrument Factory Beijing Normal University, China) was determined to be 4.76×10^{-6} Einstein L^{-1} s^{-1} under visible light irradiation (wavelength range of 400–700 nm). The incident photon flux on the photoreactor was varied by adjusting the distance between the photoreactor and the Xe arc lamp. No pH adjustment was done and the initial pH value was 7.0. The concentration of RhB was determined based on the absorption at 553.5 nm as measured by a UV–vis spectrophotometer (Lambda 40, PerkinElmer Corporation, USA). The inorganic products obtained from RhB degradation were analyzed by ion chromatograph (DX-300, Dionex Corporation, USA). The identification of RhB and its degradation intermediate products were performed by GC–MS (HP 6890 Series Gas Chromatograph (AT™ column, 20.3 m × 0.32 mm, ID of 0.25 μm)) operating at 320 °C, which was connected to HP 5973 mass selective detector, and to a flame ionization detector with H_2 as the carried gas. Intermediate products were measured by LC–MS (Thermo Quest LCQ Duo, USA, Beta Basic-C_{18} HPLC column: 150 mm × 2.1 mm, ID of 5 μm, Finnigan, Thermo, USA). Here, 20 μL of post-photocatalysis solution was injected automatically into the LC–MS system. The eluent contained 60% methanol and 40% water, and the flow rate was 0.2 mL min^{-1}. MS conditions included an electrospray ionization interface, a capillary temperature of 27 °C with a voltage of 19.00 V, a spray voltage of 5000 V and a constant sheath gas flow rate. The spectrum was acquired in the negative ion scan mode, sweeping the $m\,z^{-1}$ range from 50 to 600. Evolution of CO_2 was analyzed with an intersmat™ IGC120-MB gas chromatograph equipped with a porapack Q column (3 m in length and an inner diameter of 0.25 in.), which was connected to a catharometer detector.

The total organic carbon (TOC) concentration was determined with a TOC analyzer (TOC-5000, Shimadzu Corporation, Japan). The photonic efficiency was calculated according to the following equation [76,77]:

$$\varphi = \frac{R}{I_o}$$

where φ is the photonic efficiency (%), and R is the rate of RhB degradation (mol L^{-1} s^{-1}), and I_o is the incident photon flux (Einstein L^{-1} s^{-1}).

3. Results and discussion

3.1. Characterization

Fig. 1 presents TEM images of Gd_2YSbO_7 and Gd_2BiSbO_7, revealing nanosized particles and regular round shapes, having 20–40 nm in diameter for Gd_2YSbO_7 particle size and having 40–60 nm in diameter for Gd_2BiSbO_7 particle size. It could be seen from Fig. 1 that the mean particle size of Gd_2YSbO_7 was smaller than that of Gd_2BiSbO_7. SEM-EDS spectrum taken from the prepared Gd_2YSbO_7 indicated the presence of gadolinium, oxygen, yttrium and antimony. SEM-EDS spectrum taken from the prepared Gd_2BiSbO_7 also indicated the presence of bismuth, oxygen, gadolinium and antimony. Other elements could not be identified.

Figs. 2 and 3 present the powder X-ray diffraction patterns of Gd_2YSbO_7 and Gd_2BiSbO_7, respectively together with full-profile structure refinements of the collected data as obtained by the RIETAN™ [78] program, which is based on Rietveld analysis. The results of the final refinement for Gd_2YSbO_7 and Gd_2BiSbO_7 indicated a good agreement between the observed and calculated intensities for the pyrochlore-type structure and a cubic crystal system having a space group *Fd*3*m* (O atoms were included in the model). The lattice parameters *a* for Gd_2BiSbO_7 and Gd_2YSbO_7 were 10.70352(7) and 10.65365(1) Å, respectively. All the diffraction peaks for Gd_2YSbO_7 and Gd_2BiSbO_7 could be successfully indexed based on the lattice constant and above space group. The atomic

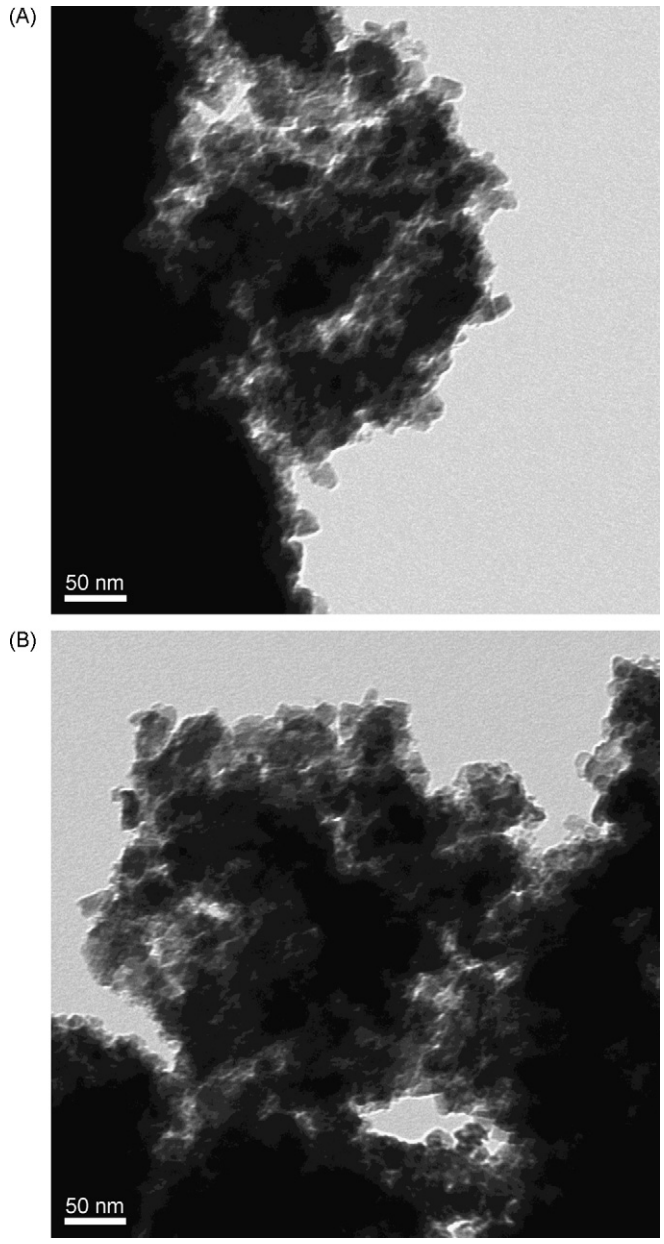

Fig. 1. TEM images of (A) Gd_2YSbO_7 and (B) Gd_2BiSbO_7.

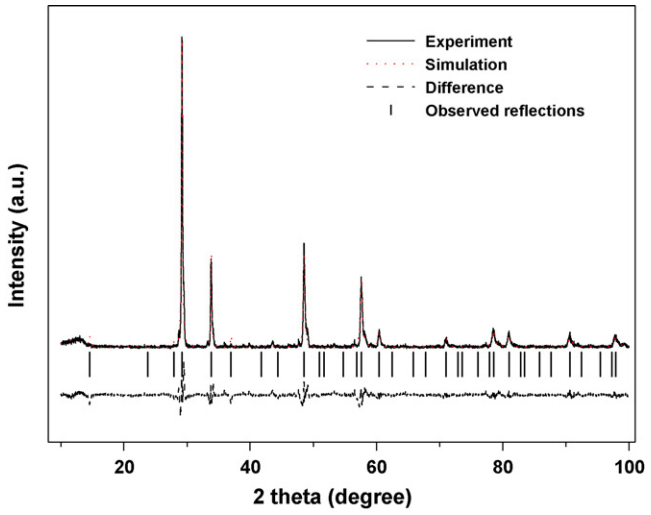

Fig. 2. X-ray powder diffraction patterns and Rietveld refinements of Gd_2YSbO_7 prepared by a solid-state reaction method at 1320 °C. A difference (observed – calculated) profile is shown beneath. The tic marks represent reflection positions.

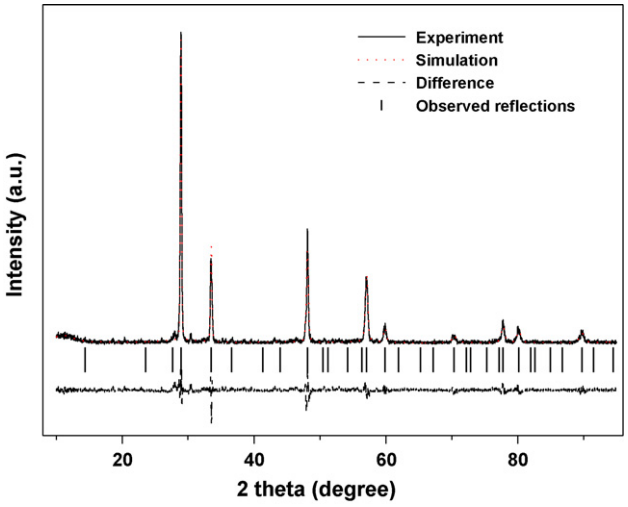

Fig. 3. X-ray powder diffraction patterns and Rietveld refinements of Gd_2BiSbO_7 prepared by a solid-state reaction method at 1040 °C. A difference (observed – calculated) profile is shown beneath. The tic marks represent reflection positions.

coordinates and structural parameters of Gd_2YSbO_7 and Gd_2BiSbO_7 are listed in Tables 1 and 2, respectively. It could be seen from Figs. 2 and 3 that not only Gd_2YSbO_7 was a single phase but also Gd_2BiSbO_7 was a single phase. In addition, Our XRD results showed that Gd_2YSbO_7 and Gd_2BiSbO_7 crystallized with the same structure, and 2θ angles of each reflection of Gd_2BiSbO_7 changed with Bi^{3+} being substituted by Y^{3+}. The lattice parameter decreased from $a = 10.70352(7)$ Å for Gd_2BiSbO_7 to $a = 10.65365(1)$ Å for Gd_2YSbO_7, which indicated a decrease for lattice parameter of the photocatalyst with decrease of the M ionic radii, Y^{3+} (1.019 Å) < Bi^{3+} (1.17 Å).

Our X-ray diffraction results showed that Gd_2YSbO_7, Gd_2BiSbO_7 and Bi_2InTaO_7 crystallized with a same pyrochlore-type structure. The cubic system structure with space group *Fd*3*m* for Bi_2InTaO_7 kept unchanged using Ta^{5+} being substituted by Sb^{5+}, In^{3+} being substituted by Bi^{3+} and Bi^{3+} being substituted by Gd^{3+}. The cubic system structure with space group *Fd*3*m* for Bi_2InTaO_7 also kept unchanged using Ta^{5+} being substituted by Sb^{5+}, In^{3+} being sub-

Table 1
Structural parameters of Gd_2YSbO_7 prepared by solid-state reaction method.

Atom	*x*	*y*	*z*	Occupation factor
Gd	0.00000	0.00000	0.00000	1.0
Y	0.50000	0.50000	0.50000	0.5
Sb	0.50000	0.50000	0.50000	0.5
O(1)	−0.16519	0.12500	0.12500	1.0
O(2)	0.12500	0.12500	0.12500	1.0

Table 2
Structural parameters of Gd_2BiSbO_7 prepared by solid-state reaction method.

Atom	*x*	*y*	*z*	Occupation factor
Gd	0.00000	0.00000	0.00000	1.0
Bi	0.50000	0.50000	0.50000	0.5
Sb	0.50000	0.50000	0.50000	0.5
O(1)	−0.14538	0.12500	0.12500	1.0
O(2)	0.12500	0.12500	0.12500	1.0

Table 3
Binding energies (BE) for key elements.

Compounds	$Bi_{4f7/2}$ BE (eV)	$Sb_{3d5/2}$ BE (eV)	$Y_{3d5/2}$ BE (eV)	$Gd_{3d5/2}$ BE (eV)	O_{1s} BE (eV)
Gd_2YSbO_7		530.90	156.80	1189.20	531.20
Gd_2BiSbO_7	159.40	530.50		1188.80	530.60

stituted by Y^{3+} and Bi^{3+} being substituted by Gd^{3+}. The outcome of refinements for Gd_2YSbO_7 generated the unweighted *R* factors, R_P = 12.16% with space group *Fd*3*m*. Similarly, the outcome of refinements for Gd_2BiSbO_7 generated the unweighted *R* factors, R_P = 12.55% with space group *Fd*3*m*. Zou et al. [14] refined the crystal structure of Bi_2InNbO_7 and obtained a large *R* factor for Bi_2InNbO_7, which was owing to a slightly modified structure model for Bi_2InNbO_7. Based on the high purity of the precursors that were used in this study and the EDS results that did not trace any other elements, it was unlikely that the observed space groups originated from the presence of impurities. Therefore, it was suggested that the slightly high *R* factors for Gd_2YSbO_7 or Gd_2BiSbO_7 were due to a slightly modified structure model for Gd_2YSbO_7 or Gd_2BiSbO_7. It should be emphasized that the defects or the disorder/order of a fraction of the atoms could result in the change of structures, including different bond-distance distributions, thermal displacement parameters and/or occupation factors for some of the atoms.

The XPS spectra of Gd_2YSbO_7 and Gd_2BiSbO_7 were measured. The various elemental peaks, corresponding to specific binding energies are given in Table 3. The results further suggested that the oxidation state of Gd, Y, Sb and O ions from Gd_2YSbO_7 was +3, +3, +5 and −2, respectively. For Gd_2YSbO_7, the average atomic ratios of Gd:Y:Sb:O, based on averaging our XPS, SEM-EDS and XFS results gave values of 2.00:0.97:1.02:6.98, respectively. Similarly, the oxidation state of Gd, Bi, Sb and O ions from Gd_2BiSbO_7 was +3, +3, +5 and −2, respectively. For Gd_2BiSbO_7, the average atomic ratios of Gd:Bi:Sb:O, based on averaging our XPS, SEM-EDS and XFS results gave values of 2.00:0.98:0.99:6.97, respectively. Hence, it could be deduced that the resulting material was of high purity under our preparation conditions. It was noteworthy that neither shoulders nor widening of any XPS peaks of the Gd_2YSbO_7 or Gd_2BiSbO_7 were observed, suggesting (albeit not proving) the absence of any other phases.

Figs. 4 and 5 present the absorption spectra of Gd_2YSbO_7 and Gd_2BiSbO_7, respectively. In contrast to the well-known TiO_2 whose absorption edge was at less than 380 nm, the newly synthesized absorption edges of Gd_2YSbO_7 and Gd_2BiSbO_7 were found to be at 479 and 499 nm, respectively, which were at the visible region of the spectrum. It was noteworthy that the apparent absorption (defined hereby as 1-transmission) could not take into consideration reflection and scattering. As a consequence, the apparent absorbance at sub-band gap wavelengths (490–700 nm for Gd_2YSbO_7, and 520–700 nm for Gd_2BiSbO_7) was higher than zero.

For a crystalline semiconductor, the optical absorption near the band edge followed the equation: [79,80] $\alpha h\nu = A(h\nu - E_g)^n$. Here, A, α, E_g and ν are proportional constant, absorption coefficient, band gap and light frequency, respectively. Within this equation, *n* determines the character of the transition in a semiconductor. E_g and *n* can be calculated by the following steps: (i) plotting $\ln(\alpha h\nu)$ versus $\ln(h\nu - E_g)$ assuming an approximate value of E_g and (ii) deducing the value of *n* based on the slope in this graph. (iii) Refining the value of E_g by plotting $(\alpha h\nu)^{1/n}$ versus $h\nu$ and extrapolating the plot to $(\alpha h\nu)^{1/n} = 0$. Based on this method, Fig. 6 shows the plot of $(\alpha h\nu)^{1/n}$ versus $h\nu$ for Gd_2YSbO_7 and Gd_2BiSbO_7. It was obviously from Fig. 6 that the value of E_g for Gd_2YSbO_7 and Gd_2BiSbO_7 was calculated to be 2.396 and 2.081 eV, respectively, while the *n* values of Gd_2YSbO_7 and Gd_2BiSbO_7 were calculated to be 0.42 and 0.48,

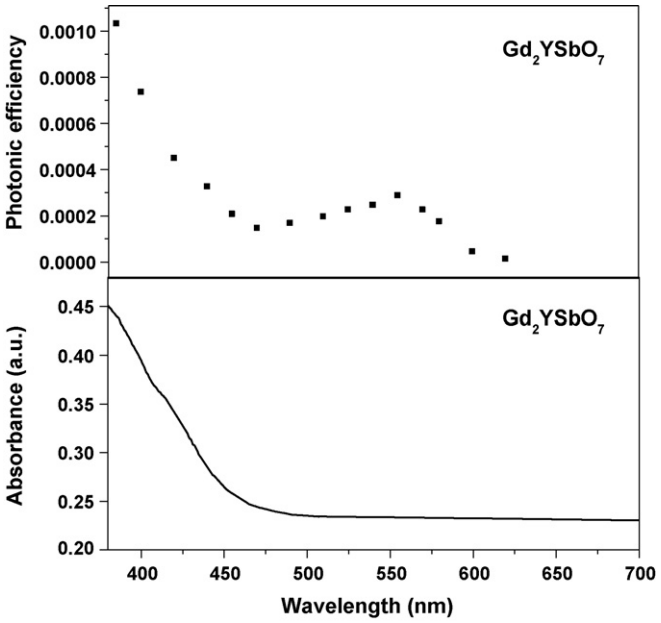

Fig. 4. Upper trace: action spectra of rhodamine B degradation with Gd_2YSbO_7 under visible light irradiation. Lower trace: absorption spectra of Gd_2YSbO_7.

respectively, indicating that Gd_2BiSbO_7 possessed narrower band gap compared with that of Gd_2YSbO_7 and the optical transition for these oxides was directly allowed.

3.2. Photocatalytic activity

In general, the process for photocatalysis by semiconductors begins with the direct absorption of supra-band gap photons and the generation of electron–hole pairs in the semiconduc-

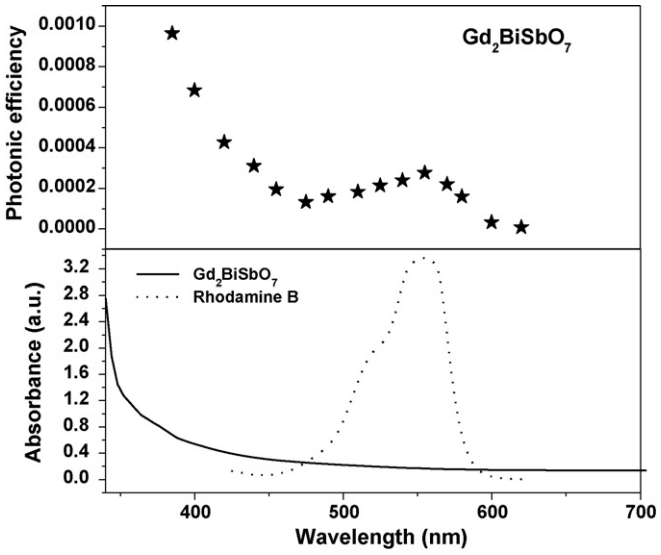

Fig. 5. Upper trace: action spectra of rhodamine B degradation with Gd_2BiSbO_7 under visible light irradiation. Lower trace: absorption spectra of Gd_2BiSbO_7 and rhodamine B.

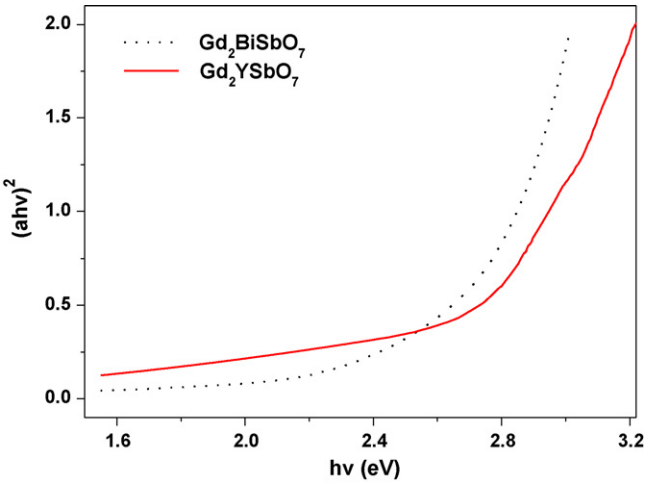

Fig. 6. Plot of $(\alpha h\nu)^2$ versus $h\nu$ for Gd_2YSbO_7 and Gd_2BiSbO_7.

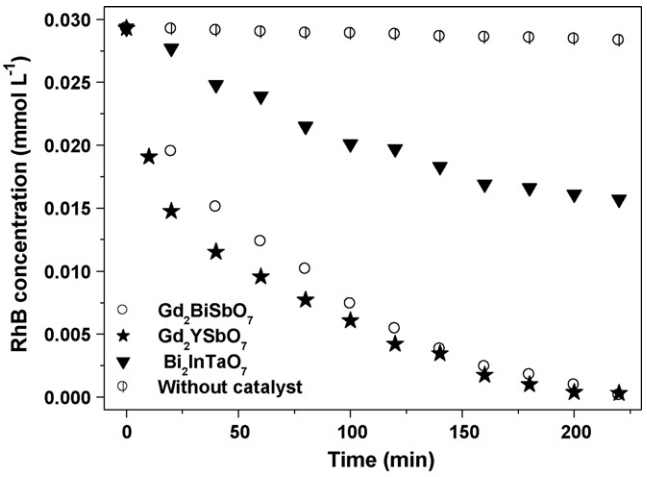

Fig. 7. Photocatalytic degradation of rhodamine B under visible light irradiation in the presence of Gd_2YSbO_7, Gd_2BiSbO_7, Bi_2InTaO_7 as well as in the absence of a photocatalyst.

tor particles. This is followed by diffusion of the charge carriers to the surface of the particle. Reduction changes in the UV–vis spectrum of rhodamine B (RhB) upon exposure to visible light ($\lambda > 400$ nm) in the presence of Gd_2YSbO_7 or Gd_2BiSbO_7 were realized, respectively. The measurements were performed under oxygen-saturation conditions ($[O_2]_{sat} = 1.02 \times 10^{-3}$ M). The degradation of RhB did not occur in the dark within Gd_2YSbO_7/RhB suspension or Gd_2BiSbO_7/RhB suspension or Bi_2InTaO_7/RhB suspension or RhB suspension. As presented in Fig. 5 typical RhB peaks at 553.5 and 525 nm are clearly noticed. A complete disappearance of the absorption signal, indicating a complete color change from deep pink into colorless solution was obtained with Gd_2YSbO_7 within 230 min and with Gd_2BiSbO_7 within 240 min. Here, the initial rate of RhB degradation was about 2.123×10^{-9} mol L^{-1} s^{-1} and the initial photonic efficiency was estimated to be 0.04460% ($\lambda = 420$ nm) for Gd_2YSbO_7. Similarly, the initial rate of RhB degradation was about 2.035×10^{-9} mol L^{-1} s^{-1} and the initial photonic efficiency was estimated to be 0.04275% ($\lambda = 420$ nm) for Gd_2BiSbO_7. In contrast, the photocatalytic efficiency with Bi_2InTaO_7 was inferior to that with Gd_2YSbO_7 or Gd_2BiSbO_7. For example, within 220 min of exposure to the visible light, the RhB concentration decreased only from 0.0293 mM to 0.0157 mM and the initial rate of RhB degradation was only 1.030×10^{-9} mol L^{-1} s^{-1}. The initial photonic efficiency was estimated to be 0.02164% ($\lambda = 420$ nm) for Bi_2InTaO_7.

The kinetics of RhB degradation under visible light irradiation was deduced based on the spectral changes and is presented in Fig. 7, which depicts the kinetics with Gd_2YSbO_7, Gd_2BiSbO_7 and Bi_2InTaO_7 as well as with the absence of a photocatalyst. As expected, reduction of RhB signal in the control measurements, taken in the absence of a photocatalyst, was pimping. In addition, the photodegradation conversion of RhB was 79.3%, 74.7% and 31.4% after visible light irradiation for 100 min with Gd_2YSbO_7, Gd_2BiSbO_7 and Bi_2InTaO_7 as catalysts, respectively. For comparison, RhB photodegradation measured by us with fluorinated titanium dioxide made according to the experimental scheme published by Ref. [56] yielded, under the same experimental conditions, no more than 59.4% of removal.

Based on above results, fast degradation rate was observed with Gd_2YSbO_7 and Gd_2BiSbO_7, and the photocatalytic degradation activity of Gd_2YSbO_7 or Gd_2BiSbO_7 was higher than that of Bi_2InTaO_7, moreover, the photocatalytic degradation activity of Gd_2YSbO_7 was a little higher than that of Gd_2BiSbO_7.

The first order nature of the photocatalytic degradation kinetics with Gd_2YSbO_7, Gd_2BiSbO_7 and Bi_2InTaO_7 is clearly demonstrated in Fig. 8, which presents a linear correlation ($R^2 > 0.99$) between $\ln(C/C_o)$ (or $\ln(TOC/TOC_o)$) and the irradiation time for the visible light photocatalytic RhB degradation at the presence of Gd_2YSbO_7, Gd_2BiSbO_7 or Bi_2InTaO_7. Here, C represents the RhB concentration at time t, and C_o represents the initial RhB concentration, and TOC represents the total organic carbon concentration at time t and TOC_o represents the initial total organic carbon concentration. According to the relationship between $\ln(C/C_o)$ and the irradia-

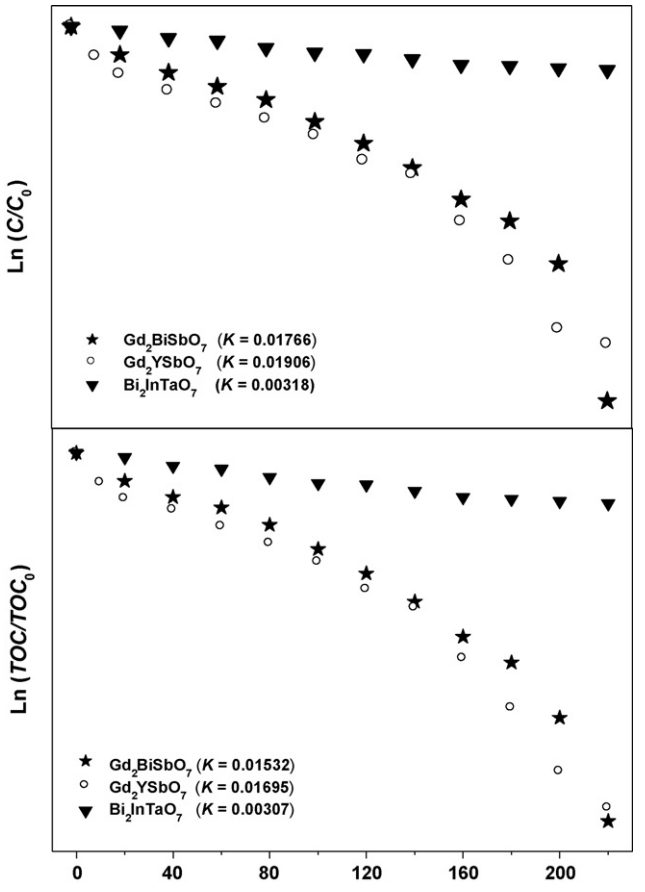

Fig. 8. Observed first-order kinetic plots for the photocatalytic rhodamine B degradation with Gd_2YSbO_7, Gd_2BiSbO_7 and Bi_2InTaO_7 under visible light irradiation.

tion time, the apparent first-order rate constant k was estimated to be 0.01906 min^{-1} with Gd_2YSbO_7, 0.01766 min^{-1} with Gd_2BiSbO_7 and 0.00318 min^{-1} with Bi_2InTaO_7, indicating that Gd_2YSbO_7 and Gd_2BiSbO_7 were more suitable than Bi_2InTaO_7 for the photocatalytic degradation of RhB under visible light irradiation, at the same time, Gd_2YSbO_7 was more suitable than Gd_2BiSbO_7 for the photocatalytic degradation of RhB under visible light irradiation. According to the relationship between $\ln(TOC/TOC_o)$ and the irradiation time, the apparent first-order rate constant k was estimated to be 0.01695 min^{-1} with Gd_2YSbO_7, 0.01532 min^{-1} with Gd_2BiSbO_7 and 0.00307 min^{-1} with Bi_2InTaO_7, indicating that the photodegradation intermediates of RhB probably appeared during the photocatalytic degradation of RhB under visible light irradiation.

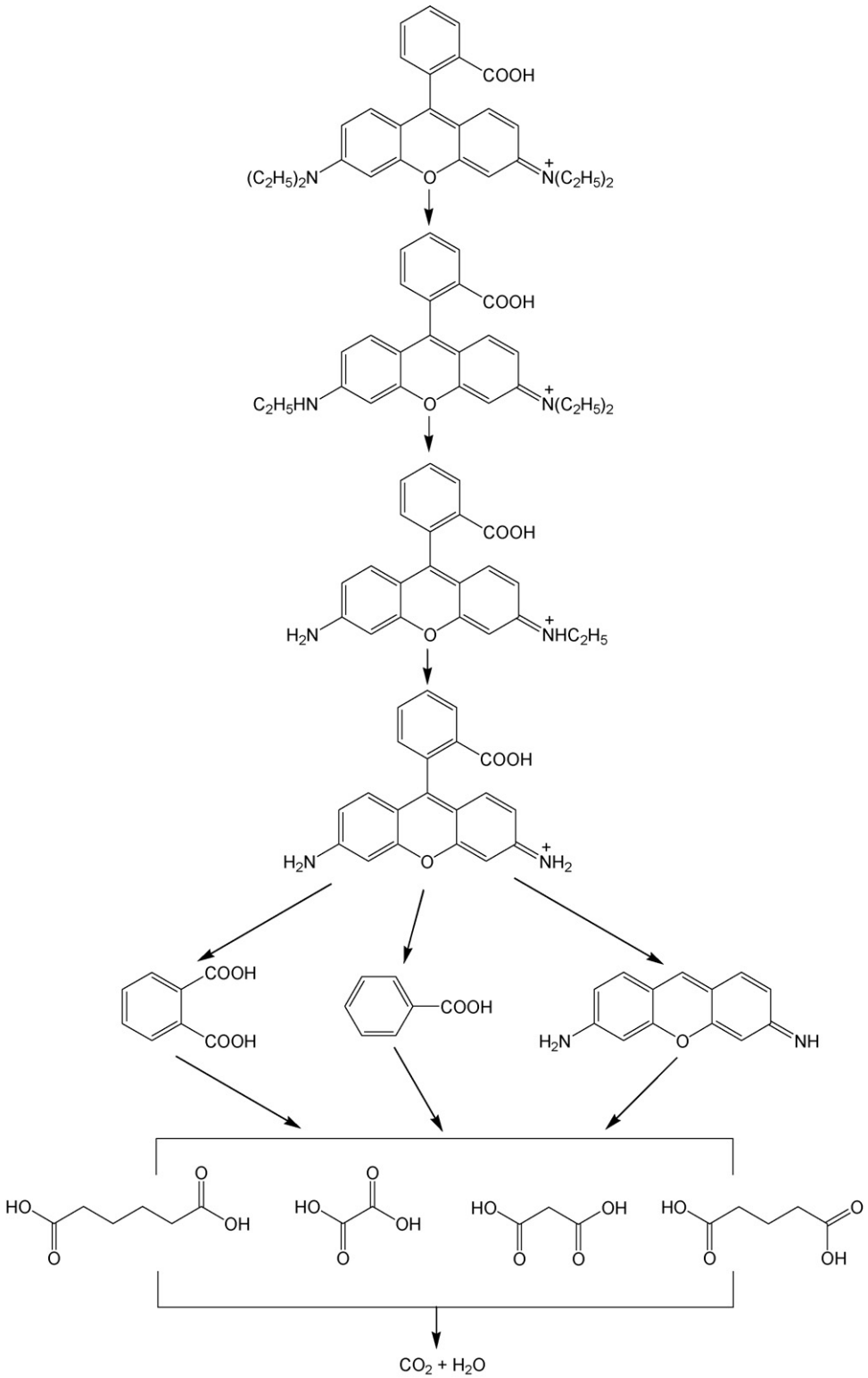

Fig. 9. Suggested photocatalytic degradation pathway scheme for rhodamine B under visible light irradiation in the presence of Gd_2YSbO_7 and Gd_2BiSbO_7.

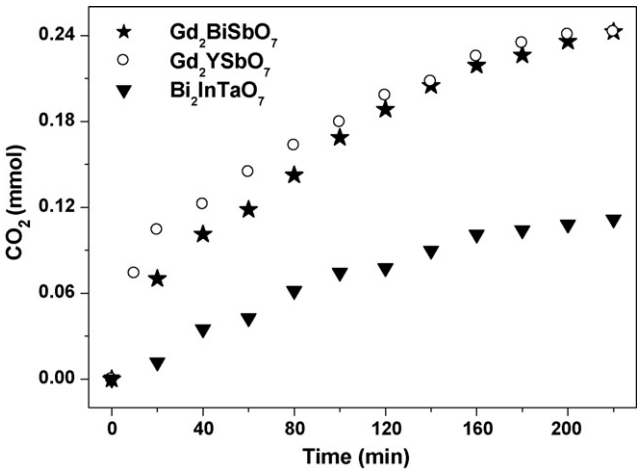

Fig. 10. CO_2 production kinetics during the photocatalytic degradation of rhodamine B with Gd_2YSbO_7, Gd_2BiSbO_7 and Bi_2InTaO_7 under visible light irradiation.

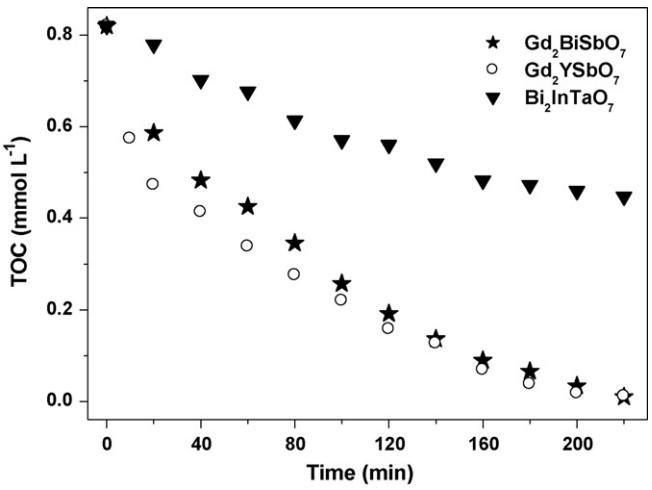

Fig. 11. Disappearance of total organic carbon (TOC) during the visible light photocatalytic degradation of rhodamine B with Gd_2YSbO_7, Gd_2BiSbO_7 and Bi_2InTaO_7.

The photodegradation intermediates of RhB in our experiment were identified as 1,2-benzenedicarboxylic acid, benzoic acid, adipic acid, oxalic acid, malonic acid and pentanedioic acid. Based on the intermediate products found in this work, a possible photocatalytic degradation pathway for RhB is proposed in Fig. 9. This pathway was similar, but not identical to the one proposed by Horikoshi et al. [81] for the photodegradation of RhB under ultraviolet light and visible light illumination assisted by microwave radiation using TiO_2 as the photocatalyst. According to Zhang et al. [75], the RhB photodegradation occurred via two competitive processes: one process was N-demethylation, and the other process was the destruction of the conjugated structure. Thus we considered that chromophore cleavage, opening-ring and mineralization would be the main photocatalytic degradation pathway of RhB in our experiment. RhB was converted to smaller organic species and ultimately was mineralized together with other organic groups to inorganic products such as CO_2 and water. Fig. 10 shows the CO_2 yield during the photocatalytic degradation of RhB with Gd_2YSbO_7, Gd_2BiSbO_7 or Bi_2InTaO_7 under visible light irradiation. The results showed that the CO_2 yield increased gradually with increasing reaction time with these three photocatalysts. The CO_2 production rate with Gd_2YSbO_7 or Gd_2BiSbO_7 was higher than the CO_2 yield with Bi_2InTaO_7, in line with the absorption curves (Figs. 4 and 5) of Gd_2YSbO_7 and Gd_2BiSbO_7. For example, the CO_2 production following visible light irradiation for 200 min was 0.2407 mmol with Gd_2YSbO_7, 0.2359 mmol with Gd_2BiSbO_7 and 0.1080 mmol with Bi_2InTaO_7.

Total organic carbon (TOC) measurements (Fig. 11) revealed segmental disappearance of organic carbon within 220 min of exposure of a solution containing Gd_2YSbO_7 or Gd_2BiSbO_7 or Bi_2InTaO_7. The results showed that 73.16% or 68.60% or 30.47% of TOC decrease was obtained after visible light irradiation for 100 min with Gd_2YSbO_7 or Gd_2BiSbO_7 or Bi_2InTaO_7 as a photocatalyst. In succession, the complete mineralization of RhB with Gd_2YSbO_7 or Gd_2BiSbO_7 as the photocatalyst was achieved after 245 min irradiation or 260 min irradiation due to the decrease of the TOC (100%). The turnover numbers (the ratio between total amount of evolved gas and catalyst that was used) after 60 h of reaction time under visible light irradiation were calculated to be (with addition of 0.00879 mmol additional RhB in the solution after every 6 h irradiation) more than 1.12 and 1.01 for Gd_2YSbO_7 and Gd_2BiSbO_7, respectively. These turnover numbers were enough to prove that the reactions occurred catalytically. The reactions stopped when the light was turned off in this experiment, showing the obvious light response.

The photocatalytic performance of the new compounds Gd_2YSbO_7 and Gd_2BiSbO_7, under visible light irradiation was remarkable. This superior quality can be even more appreciated if one considers the fact that the specific surface area of these compounds is by far smaller than that of titanium dioxide. Here, BET isotherm measurements of the three compounds gave a specific surface area of $1.28\,m^2\,g^{-1}$, $1.17\,m^2\,g^{-1}$ and $1.26\,m^2\,g^{-1}$ for Gd_2YSbO_7, Gd_2BiSbO_7 and Bi_2InTaO_7, respectively, which was almost 36 times smaller than that of TiO_2 which was measured to be $46.24\,m^2\,g^{-1}$.

As depicted in Fig. 7, some decrease in the RhB UV–vis absorbance signal was obtained under visible light irradiation even in the absence of a photocatalyst. Here, the initial rate of RhB degradation was estimated to be $0.074 \times 10^{-9}\,mol\,L^{-1}\,s^{-1}$ and the photonic efficiency averaged after 220 min of exposure was 0.00155% ($\lambda = 420$ nm). It was suggested that the observed disappearance of RhB in the absence of a photocatalyst was due to direct dye-sensitization, which was similar to the observation of Zhao et al. [82] regarding alizarin red and X3B dyes.

Figs. 4 and 5 show the action spectra of RhB degradation in the presence of Gd_2YSbO_7 and Gd_2BiSbO_7 under visible light irradiation. A clear photonic efficiency (0.02855% at its maximal point) at wavelengths which corresponded to sub-E_g energies of the photocatalysts (λ from 479 nm to 700 nm) was observed for Gd_2YSbO_7 and Gd_2BiSbO_7. The existence of photonic efficiency at energies where no photons were absorbed by the photocatalysts, and in particular the correlation between the low-energy action spectrum and the absorption spectrum of RhB, clearly demonstrated that any photodegradation at wavelengths above 479 nm should be attributed to photosensitization by the dye RhB itself (Scheme I):

$$\text{Scheme I}: \ RhB_{(ads)} \xrightarrow{\text{Visible light}} RhB^*_{(ads)} \quad (1)$$

$$RhB^*_{(ads)} + Gd_2YSbO_7\,(\text{or}\,Gd_2BiSbO_7) \rightarrow Gd_2YSbO_7\,(\text{or}\,Gd_2BiSbO_7)(e) + RhB^+_{(ads)} \quad (2)$$

$$Gd_2YSbO_7\ (\text{or}\ Gd_2BiSbO_7)\ (e) + O_2 \rightarrow Gd_2YSbO_7\ (\text{or}\ Gd_2BiSbO_7) + {}^{\bullet}O_2^- \quad (3)$$

According to this mechanism, RhB adsorbed on Gd_2YSbO_7 or Gd_2BiSbO_7 is excited by visible light irradiation. An electron is then injected from the excited RhB to the conduction band of Gd_2YSbO_7 or Gd_2BiSbO_7 where the electron is scavenged by molecular oxygen. Scheme I serves to explain the results obtained with Gd_2YSbO_7

or Gd_2BiSbO_7 under visible light irradiation, where Gd_2YSbO_7 or Gd_2BiSbO_7 may serve at most to reduce recombination of electrons and holes via the scavenging of electrons [83].

The situation was different below 479 nm, where the photonic efficiency correlated well with the absorption spectra of Gd_2YSbO_7 and Gd_2BiSbO_7. This evidently showed that the mechanism which was responsible for the photodegradation of RhB went through band gap excitation of Gd_2YSbO_7 and Gd_2BiSbO_7. Although detailed experiments about the effect of oxygen and water on the degradation scheme were not performed, it was sensible to assume that the mechanism in the first steps was similar to the one observed for Gd_2YSbO_7 or Gd_2BiSbO_7 under supra-band gap irradiation, namely (Scheme II):

Scheme II : $Gd_2YSbO_7\,(\text{or}\,Gd_2BiSbO_7) \xrightarrow{\text{Visible light}} h^+ + e^-$ (4)

$$e^- + O_2 \rightarrow {}^{\bullet}O_2^- \quad (5)$$

$$h^+ + OH^- \rightarrow {}^{\bullet}OH \quad (6)$$

Previous luminescence studies have shown that the closer the M–O–M bond angle is to 180°, the more delocalized is the excited state [84], and the charge carriers can move easily in the matrix. The mobility of the photoinduced electrons and holes influences the photocatalytic activity because high diffusivity increases the probability that the photogenerated electrons and holes will reach reactive sites on the catalyst surface. Based on above results, the lattice parameter $a = 10.65365(1)$ Å for Gd_2YSbO_7 was smaller than the lattice parameter $a = 10.70352(7)$ Å for Gd_2BiSbO_7, thus the photoinduced electrons and holes inside Gd_2YSbO_7 were easier and faster to reach the reactive sites on the catalyst surface compared with those of Gd_2BiSbO_7, as a result, the photocatalytic degradation activity of Gd_2YSbO_7 was higher than that of Gd_2BiSbO_7. In this experiment, the Y–O–Sb bond angle was 136.795° and the Bi–O–Sb bond angle was 118.764°, indicating that the Y–O–Sb or Bi–O–Sb bond angle was close to 180°. Thus the photocatalytic activity of Gd_2YSbO_7 or Gd_2BiSbO_7 was accordingly higher. The crystal structures of Gd_2YSbO_7, Gd_2BiSbO_7 and Bi_2InTaO_7 were the same, but their electronic structures were considered to be a little different. For Gd_2YSbO_7 or Gd_2BiSbO_7, Sb was 5*p*-block metal element, and Gd was 5*d*-block rare earth metal element, and Y was 4*d*-block metal element, but for Bi_2InTaO_7, Ta was 5*d*-block metal element, indicating that the photocatalytic activity might be affected by not only the crystal structure but also the electronic structure of the photocatalysts. Based on above analysis, the difference of photocatalytic degradation of RhB among Gd_2YSbO_7, Gd_2BiSbO_7 and Bi_2InTaO_7 could be attributed mainly to the difference in their crystalline and electronic structure.

Fig. 12 shows the suggested band structures of Gd_2YSbO_7 and Gd_2BiSbO_7. Recently, the electronic structures of $InMO_4$ (M = V, Nb and Ta) and $BiVO_4$ were reported by Oshikiri et al. based on the first principle calculations [85]. The conduction bands of $InMO_4$ (M = V, Nb and Ta) were mainly composed of a dominant *d* orbital component from V 3*d*, Nb 4*d* and Ta 5*d* orbitals, respectively. The valence bands of the $BiVO_4$ photocatalyst were composed of a small Bi 6*s* orbital component and a dominant O 2*p* orbital component. The band structures of Gd_2YSbO_7 and Gd_2BiSbO_7 should be similar to $InMO_4$ (M = V, Nb and Ta) and $BiVO_4$. Therefore, we concluded that the conduction band of Gd_2YSbO_7 was composed of Gd 5*d*, Y 4*d* and Sb 5*p* orbital component and the valence band of Gd_2YSbO_7 was composed of a small dominant O 2*p* orbital component. Similarly, the conduction band of Gd_2BiSbO_7 was composed of Gd 5*d* and Sb 5*p* orbital component. The valence band of Gd_2BiSbO_7 was composed of a small Bi 6*s* orbital component and a dominant O 2*p* orbital component. Direct absorption of photons by Gd_2YSbO_7 or Gd_2BiSbO_7 could produce electron–hole pairs in the catalyst, indicating that the larger energy than the band gap was necessary for decomposing RhB by photocatalysis.

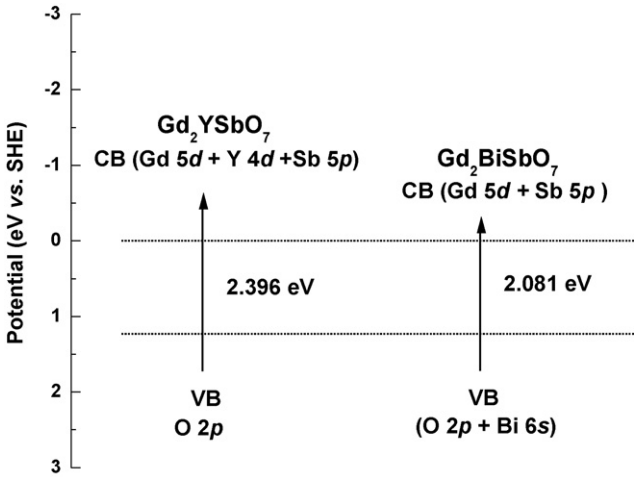

Fig. 12. Suggested band structures of Gd_2YSbO_7 and Gd_2BiSbO_7.

The presented results indicated that Gd_2YSbO_7 (or Gd_2BiSbO_7)/(visible light) photocatalysis might be regarded as a method for practical treatment of diluted colored wastewater. Our Gd_2YSbO_7 (or Gd_2BiSbO_7)/(visible light) photocatalysis system could be utilized for decolorization, purification and detoxification in textile industries and printing and dyeing industries in semi-arid countries. We designed Gd_2YSbO_7 (or Gd_2BiSbO_7)/(visible light) photocatalysis system without demanding chemical reagents or using high pressure of oxygen or heating. The decolorized and detoxified water were submitted to our new system for treatment and the results showed that the Gd_2YSbO_7 (or Gd_2BiSbO_7)/(visible light) photocatalysis system might provide a valuable treatment for purifying and reusing colored aqueous effluents.

4. Conclusions

Gd_2YSbO_7 and Gd_2BiSbO_7 were prepared by solid-state reaction method for the first time. The structural, optical absorption and visible light photocatalytic properties of Gd_2YSbO_7 and Gd_2BiSbO_7 were investigated and compared with that of Bi_2InTaO_7. XRD results indicated that Gd_2YSbO_7 and Gd_2BiSbO_7 crystallized with the pyrochlore-type structure and cubic crystal system (space group *Fd*3*m*). The lattice parameters of Gd_2YSbO_7 and Gd_2BiSbO_7 were found to be $a = 10.65365(1)$ Å and $a = 10.70352(7)$ Å. The band gaps of Gd_2YSbO_7 and Gd_2BiSbO_7 were estimated to be about 2.396 and 2.081 eV such that Gd_2YSbO_7 or Gd_2BiSbO_7 showed a strong optical absorption in the visible light region ($\lambda > 400$ nm). Photocatalytic decomposition of aqueous solutions of RhB were observed under visible light irradiation in the presence of Gd_2YSbO_7 or Gd_2BiSbO_7 accompanied with the formation of end products such as carbon dioxide and water. Complete removal of carbon was obtained as indicated from TOC measurements with Gd_2YSbO_7 or Gd_2BiSbO_7 as a catalyst. Hence it could be concluded that Gd_2YSbO_7 (or Gd_2BiSbO_7)/vis system might be regarded as an effective way for treating of textile industry wastewater. Gd_2YSbO_7 or Gd_2BiSbO_7 also showed higher photocatalytic activity compared with Bi_2InTaO_7 for RhB photocatalytic degradation under visible light irradiation. The photocatalytic RhB degradation followed the first-order reaction kinetics. The apparent first-order rate constant k was 0.01906, 0.01766 or 0.00318 min^{-1} with Gd_2YSbO_7, Gd_2BiSbO_7 or Bi_2InTaO_7 as a catalyst. The possible photocatalytic degradation pathway of RhB was revealed under visible light irradiation.

Acknowledgements

This work was supported by the National Natural Science Foundation of China (No. 20877040). This work was supported by a grant from the Technological Supporting Foundation of Jiangsu Province (No. BE2009144). This work was supported by a grant from the Natural Science Foundation of Jiangsu Province (Nos. BK2007717, BK2006130).

References

[1] A. Fujishima, K. Honda, Nature 238 (1972) 37–38.
[2] C.E. Houlden, C.D. Bailey, J.G. Ford, M.R. Gagne, G.C. Lloyd-Jones, K.I. Booker-Milburn, J. Am. Chem. Soc. 130 (1998) 10066–10067.
[3] S.Y. Chai, Y.J. Kim, M.H. Jung, A.K. Chakraborty, D. Jung, W.I. Lee, J. Catal. 262 (2009) 144–149.
[4] P.L. Zhang, S. Yin, T. Sato, Appl. Catal. B 89 (2009) 118–122.
[5] X.W. Zhang, L.C. Lei, J.L. Zhang, Q.X. Chen, J.G. Bao, B. Fang, Sep. Purif. Technol. 66 (2009) 417–421.
[6] L.M. Song, S.J. Zhang, B. Chen, Catal. Commun. 10 (2009) 1565–1568.
[7] K.A. Koyano, T. Tatsumi, Micropor. Mater. 10 (1997) 259–271.
[8] P. Raja, V. Nadtochenko, U. Klehm, J. Kiwi, Appl. Catal. B 81 (2008) 258–266.
[9] I.C. Kang, Q. Zhang, S. Yin, T. Sato, F. Saito, Appl. Catal. B 84 (2008) 570–576.
[10] D.Z. Li, Z.X. Chen, Y.L. Chen, W.J. Li, H.J. Huang, Y.H. He, X.Z. Fu, Environ. Sci. Technol. 42 (2008) 2130–2135.
[11] W.F. Yao, J.H. Ye, Chem. Phys. Lett. 111 (2007) 18348–18352.
[12] M. Kitano, M. Takeuchi, M. Matsuoka, J.M. Thomas, M. Anpo, Chem. Lett. 34 (2005) 616–617.
[13] M. Anpo, H. Yamashita, K. Ikeue, Y. Fujii, S.G. Zhang, Y. Ichihashi, D.R. Park, Y. Suzuki, K. Koyano, T. Tatsumi, Catal. Today 44 (1998) 327–332.
[14] Z.G. Zou, J.H. Ye, H. Arakawa, J. Mater. Sci. Lett. 19 (2000) 1909–1911.
[15] B. Neppolian, H. Yamashita, Y. Okada, H. Nishijima, M. Anpo, Catal. Lett. 105 (2005) 111–117.
[16] D.K. Lee, J.I. Jeon, M.H. Kim, W. Choi, H.I. Yoo, J. Solid State Chem. 178 (2005) 185–193.
[17] J.F. Luan, Z.G. Zou, M.H. Lu, S.R. Zheng, Y.F. Chen, J. Cryst. Growth 273 (2004) 241–247.
[18] H. Yoshitake, T. Sugihara, T. Tatsumi, Chem. Mater. 14 (2002) 1023–1029.
[19] M. Anpo, M. Takeuchi, J. Catal. 216 (2003) 505–516.
[20] Z.G. Zou, J.H. Ye, K. Sayama, H. Arakawa, Nature 414 (2001) 625–627.
[21] Y.V. Meteleva, F. Roessner, G.F. Novikov, J. Photochem. Photobiol. A 196 (2008) 154–158.
[22] A. Dodd, A. McKinley, T. Tsuzuki, M. Saunders, J. Phys. Chem. Solids 68 (2007) 2341–2348.
[23] M. Kompitsas, A. Giannoudakos, E. György, G. Sauthier, A. Figueras, I.N. Mihailescu, Thin Solid Films 515 (2007) 8582–8585.
[24] B. Neppolian, Q.L. Wang, H. Yamashita, H. Choi, Appl. Catal. A 333 (2007) 264–271.
[25] G.P. Wu, T. Chen, W.G. Su, G.H. Zhou, X. Zong, Z.B. Lei, C. Li, Int. J. Hydrogen Energy 33 (2008) 1243–1251.
[26] G.P. Wu, T. Chen, X. Zong, H.J. Yan, G.J. Ma, X.L. Wang, Q. Xu, D.G. Wang, Z.B. Lei, C. Li, J. Catal. 253 (2008) 225–227.
[27] H.B. Fu, C.S. Pan, W.Q. Yao, Y.F. Zhu, J. Phys. Chem. B 109 (2005) 22432–22439.
[28] R. Dholam, N. Patel, M. Adami, A. Miotello, Int. J. Hydrogen Energy 34 (2009) 5337–5346.
[29] W.D. Yang, C.S. Hsieh, T.Y. Wei, Z.J. Chung, I.L. Huang, J. Nanosci. Nanotechnol. 9 (2009) 3843–3847.
[30] H. Kunkely, A. Vogler, Angew. Chem. Int. Ed. 48 (2009) 1685–1687.
[31] Y.P. Yuan, X.L. Zhang, L.F. Liu, X.J. Jiang, J. Lv, Z.S. Li, Z.G. Zou, Int. J. Hydrogen Energy 33 (2008) 5941–5946.
[32] K. Maeda, H. Terashima, K. Kase, M. Higashi, M. Tabata, K. Domen, Bull. Chem. Soc. Jpn. 81 (2008) 927–937.
[33] C.C. Hu, J.N. Nian, H. Teng, Sol. Energy Mater. Sol. Cells 92 (2008) 1071–1076.
[34] Y. Lee, H. Terashima, Y. Shimodaira, K. Teramura, M. Hara, H. Kobayashi, K. Domen, M. Yashima, J. Phys. Chem. C 111 (2007) 1042–1048.
[35] Y.G. Lee, K. Teramura, M. Hara, K. Domen, Chem. Mater. 19 (2007) 2120–2127.
[36] K.L. Bray, G.C. Lloyd-Jones, M.P. Munoz, P.A. Slatford, E.H.P. Tan, A.R. Tyler-Mahon, P.A. Worthington, Chem. Eur. J. 12 (2006) 8650–8663.
[37] D.L. Jiang, S.Q. Zhang, H.J. Zhao, Environ. Sci. Technol. 41 (2007) 303–308.
[38] C. Kim, S.J. Doh, S.G. Lee, S.J. Lee, H.Y. Kim, Appl. Catal. A 330 (2007) 127–133.
[39] F.N. Chen, X.D. Yang, F.F. Xu, Q. Wu, Y.P. Zhang, Environ. Sci. Technol. 43 (2009) 1180–1184.
[40] Z.C. Shan, W.D. Wang, X.P. Lin, H.M. Ding, F.Q. Huang, J. Solid State Chem. 181 (2008) 1361–1366.
[41] G.C. Lloyd-Jones, Org. Biomol. Chem. 1 (2003) 215–236.
[42] J. Singh, S. Uma, J. Phys. Chem. C 113 (2009) 12483–12488.
[43] L.A.T. Espinoza, E. ter Haseborg, M. Weber, F.H. Frimmel, Appl. Catal. B 87 (2009) 56–62.
[44] J.F. Luan, B.C. Pan, Y. Paz, Y.M. Li, X.S. Wu, Z.G. Zou, Phys. Chem. Chem. Phys. 11 (2009) 6289–6298.
[45] J.F. Luan, W. Zhao, J.W. Feng, H.L. Cai, Z. Zheng, B.C. Pan, X.S. Wu, Z.G. Zou, Y.M. Li, J. Hazard. Mater. 164 (2009) 781–789.
[46] D. Fabbri, A.B. Prevot, V. Zelano, M. Ginepro, E. Pramauro, Chemosphere 71 (2008) 59–65.
[47] J.F. Luan, Z. Zheng, X.S. Wu, G.Y. Luan, Z.G. Zou, Mater. Res. Bull. 43 (2008) 3332–3344.
[48] Q. Wang, C.C. Chen, D. Zhao, W.H. Ma, J.C. Zhao, Langmuir 24 (2008) 7338–7345.
[49] W. Bahnemann, M. Muneer, M.M. Haque, Catal. Today 124 (2007) 133–148.
[50] G.L.J. Bar, G.C. Lloyd-Jones, K.I. Booker-Milburn, J. Am. Chem. Soc. 127 (2005) 7308–7309.
[51] J. Marugan, D. Hufschmidt, M.J. Lopez-Munoz, V. Selzer, D.W. Bahnemann, Appl. Catal. B 62 (2006) 201–207.
[52] L. Ciabini, M. Santoro, R. Bini, V. Schettino, Phys. Rev. Lett. 88 (2002), 085505-1–085505-4.
[53] M. Muneer, D.W. Bahnemann, M. Qamar, M.A. Tariq, M. Faisal, Appl. Catal. A 289 (2005) 224–230.
[54] R.S. Sonawane, M.K. Dongare, J. Mol. Catal. A 243 (2006) 68–76.
[55] M.M. Haque, M. Muneer, D.W. Bahnemann, Environ. Sci. Technol. 40 (2006) 4765–4770.
[56] G.S. Rao, F.R. Fan, G.F. Wang, Z.X. Wu, F. Yi, Q.L. Zhong, B. Ren, Z.Q. Tian, Acta Phys. -Chim. Sin. 24 (2008) 345–349.
[57] J.W. Tang, J.H. Ye, Chem. Phys. Lett. 410 (2005) 104–107.
[58] Y. Liu, Z.B. Wei, Z.C. Feng, M.F. Luo, P.L. Ying, C. Li, J. Catal. 202 (2001) 200–204.
[59] D. Chatterjee, S. Dasgupta, J. Photochem. Photobiol. C 6 (2005) 186–205.
[60] G. Granados, C.A. Paez, F. Martinez, E.A. Paez-Mozo, Catal. Today 107 (2005) 589–594.
[61] S.F. Chen, Y.Z. Liu, Chemosphere 67 (2007) 1010–1017.
[62] H. Yoshitake, T. Sugihara, T. Tatsumi, Phys. Chem. Chem. Phys. 5 (2003) 767–772.
[63] T. Fujii, H. Nishikiori, T. Tamura, Chem. Phys. Lett. 233 (1995) 424–429.
[64] O. Valdes-Aguilera, D.C. Neckers, Accounts Chem. Res. 22 (1989) 171–177.
[65] S. Horikoshi, F. Hojo, H. Hikaka, N. Serpone, Environ. Sci. Technol. 38 (2004) 2198–2208.
[66] M. Asilturk, F. Sayilkan, S. Erdemoglu, M. Akarsu, H. Sayilkan, M. Erdemoglu, E. Arpac, J. Hazard. Mater. 129 (2006) 164–170.
[67] S. Horikoshi, H. Hidaka, N. Serpone, Environ. Sci. Technol. 36 (2002) 1357–1366.
[68] J.M. Wu, T.W. Zhang, J. Photochem. Photobiol. A 162 (2004) 171–177.
[69] J.M. Wu, Environ. Sci. Technol. 41 (2007) 1723–1728.
[70] J.Q. Li, L.P. Li, L. Zheng, Y.Z. Xian, L.T. Jin, Electrochim. Acta 51 (2006) 4942–4949.
[71] X. Li, J.H. Ye, J. Phys. Chem. C 111 (2007) 13109–13116.
[72] J.Y. Li, W.H. Ma, P.X. Lei, J.C. Zhao, J. Environ. Sci.-China 19 (2007) 892–896.
[73] T.X. Wu, G.M. Liu, J.C. Zhao, H. Hidaka, N. Serpone, J. Phys. Chem. B 102 (1998) 5845–5851.
[74] J.C. Zhao, T.X. Wu, K.Q. Wu, K. Oikawa, H. Hidaka, N. Serpone, Environ. Sci. Technol. 32 (1998) 2394–2400.
[75] J.P. Li, X. Zhang, Z.H. Ai, F.L. Jia, L.Z. Zhang, J. Lin, J. Phys. Chem. C 111 (2007) 6832–6836.
[76] J. Marugán, D. Hufschmidt, G. Sagawe, V. Selzer, D. Bahnemann, Water Res. 40 (2006) 833–839.
[77] S. Sakthivel, M.V. Shankar, M. Palanichamy, B. Arabindoo, D.W. Bahnemann, V. Murugesan, Water Res. 38 (2004) 3001–3008.
[78] F. Izumi, J. Crystallogr. Assoc. Jpn. 27 (1985) 23–26.
[79] J. Tauc, R. Grigorovici, A. Vancu, Phys. Status Solidi 15 (1966) 627–637.
[80] M.A. Butler, J. Appl. Phys. 48 (1977) 1914–1920.
[81] S. Horikoshi, A. Saitou, H. Hidaka, N. Serpone, Environ. Sci. Technol. 37 (2003) 5813–5822.
[82] G. Liu, T. Wu, J. Zhao, H. Hidaka, N. Serpone, Environ. Sci. Technol. 33 (1999) 2081–2087.
[83] C. Nasr, K. Vinodgopal, L. Fisher, S. Hotchandani, A.K. Chattopadhyay, P.V. Kamat, J. Phys. Chem. 100 (1996) 8436–8442.
[84] M. Wiegel, W. Middel, G. Blasse, J. Mater. Chem. 5 (1995) 981–983.
[85] M. Oshikiri, M. Boero, J.H. Ye, Z.G. Zou, G. Kido, J. Chem. Phys. 117 (2002) 7313–7318.